Electrochimica Acta 235 (2017) 304–310

Contents lists available at ScienceDirect

Electrochimica Acta

journal homepage: www.elsevier.com/locate/electacta

Zinc terephthalates $ZnC_8H_4O_4$ as anodes for lithium ion batteries

Liping Wang[a,*], Jian Zou[a], Shulin Chen[b,c], Jingyi Yang[a], Fangzhu Qing[a], Peng Gao[b,d], Jingze Li[a,*]

[a] State Key Laboratory of Electronic Thin Films and Integrated Devices, University of Electronic Science and Technology of China, Chengdu 610054, China
[b] Electron Microscopy Laboratory, School of Physics, Peking University, Beijing 100871, China
[c] State Key Laboratory of Advanced Welding and Joining, Harbin Institute of Technology, Harbin 150001, China
[d] Collaborative Innovation Center of Quantum Matter, Beijing 100871, China

ARTICLE INFO

Article history:
Received 13 January 2017
Received in revised form 23 February 2017
Accepted 13 March 2017
Available online 18 March 2017

Keywords:
Amorphous
Carbonyl compounds
Organic electrodes
Zinc terephthalate
Metal organic framework

ABSTRACT

Organic materials offer the advantages of cost-effective, environmental benignity, and molecular structural diversity as applications of electrode materials for lithium ion batteries. In fact, their lithium storage behaviors in terms of dynamics and kinetics intrinsically lie in ion migration in solids. Thus the solid forms including crystalline and amorphous states are crucial for the properties. In this study, a conventional carbonyl type organic material, namely zinc terephthalate ($ZnC_8H_4O_4$), is obtained in both well-crystalline and amorphous forms and applied as anodes for lithium ion batteries. $ZnC_8H_4O_4$ with amorphous structure shows higher lithium storage capacity and better capacity retention compared with that of crystalline one. It is ascribed that the amorphous phase provides a higher lithium ion diffusion coefficient than the crystalline one under the conditions of similar electronic conductivity.

1. Introduction

Lithium ion batteries outperform other rechargeable batteries (e.g. Ni-MH, Pb-acid, vanadium redox) in terms of energy density and power density, which makes them to dominate the markets of portable electronics and provides the opportunities of applications in electric vehicles and grid [1]. Pursuit of electrode materials with low-cost, environmental friendly and sustainability is one of the main targets. Fortunately, organic electrode materials cater for these requirements. Various organic compounds including carbonyl compounds, organiosulfur compounds, free radical compounds, conjugated redox polymers have been reported as cathodes or anodes via the mechanisms of "chemical bonding" and electron rearrangements [2–7]. Among them, carbonyl compounds are ideal organic anodes due to their moderate operational voltage of 0.8 V vs. Li^+/Li, which can effectively avoid the decomposition of conventional carbonate-based electrolytes [8,9]. Scheme 1 shows the lithium storage mechanism of one representative carbonyl compounds, i.e. terephthalates, in which the carbonyl functional groups absorb Li^+ and the electrons rearrange in the conjugated π-bond of the benzene and —COO— groups for the discharge process, and vice versa for the charging process.

The mechanism mentioned above gives a good explanation for the lithium storage behavior in its theoretical capacity and addresses the importance of electronic structure. Thus, it seems that the charge-transfer plays a crucial role in the lithium storage mechanism. Nevertheless, lithium ions have to pass through the solids of the electrodes from a microstructure point of view during the discharge-charge process, which is actually the rate-determine process [10]. Thus understanding the ion transport properties in the solid phase is crucial for its electrochemical performance. According to the state-of-the-art, various attentions have been devoted to the relations between phases and performance [11]. MnO_2 polymorphs with different crystalline forms demonstrated distinct electrochemical behaviors not only capacities but also operational voltages [12,13]. Alkaline terephthalates, for example, $Li_2C_8H_4O_4$ and $K_2C_8H_4O_4$ with similar molecular structures and functional groups but different crystallography presented similar operational voltage profile as anodes for lithium ion batteries, but quite different rate performance because the latter one has a two-dimensional lithium ion diffusion route rather than one dimension route of $Li_2C_8H_4O_4$-type [14]. Moreover, it is interesting to find that amorphous phase $FePO_4$ demonstrated a capacity of 140 mAh g^{-1} as cathodes while the trigonal quartz phase $FePO_4$ was almost

* Corresponding authors. Tel.: +86 28 83207620; Fax: +86 28 83202569.
E-mail addresses: lipingwang@uestc.edu.cn (L. Wang), lijingze@uestc.edu.cn (J. Li).

http://dx.doi.org/10.1016/j.electacta.2017.03.095
0013-4686/

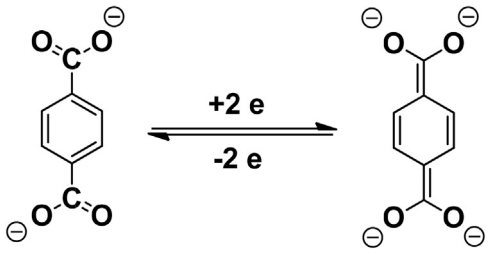

Scheme 1. Lithium storage mechanisms for the terephthalates.

electrochemical inert [15]. It is suspected that the amorphous phase gives a glassy form with isotropic nature that is favorable for lithium migration, whereas the crystalline $FePO_4$ is too crowded for the lithium ion to pass through its periodic rigid and robust "atom cages". Therefore, understanding the phase structure is essential to mechanistic study and is helpful to further engineer to improve its corresponding electrochemical properties.

In our previous study, we have synthesized a series of metal terephthalates $MC_8H_4O_4$ (M = Li_2, K_2, Ag_2, Mg, Ca, Ba, Sr, Co) [16–21]. It is interesting to find that cation varieties contribute a great difference in physic-chemical properties. Substitution of Li^+ with Ca^{2+} can improve the thermal stability and alleviate the solubility in the electrolytes so as to enhance the cycling performance. Introducing of Co cation gives a multiple-electron transfer with a capacity of more than 600 mAh g^{-1}. Alkaline earth metal cation-type $MC_8H_4O_4$ (M = Ca, Sr, Ba) bring in different crystallography in which $SrC_8H_4O_4$ has the worst capacity retention behavior due to unstable structure of the highly distorted Sr-O octahedron. In this work, we focus on a new carbonyl-type organic material, zinc terephthalate ($ZnC_8H_4O_4$), which is also a representative metal-organic framework material and can be easily synthesized. Both of its crystalline form and amorphous form are obtained. Their lithium storage behaviors are systematically studied. Although both of them have comparable electronic conductivity at a magnitude of 10^{-7} S m^{-1}, amorphous phase displays higher capacity and better capacity retention compared with that of crystalline phase as a consequence of a higher lithium diffusion coefficient in the solids.

2. Experimental section

2.1. Materials synthesis

The preparation of zinc terephthalate (denoted as ZnTPA·$2H_2O$) was synthesized by a facile displacement reaction, similar to our previous synthesis of $MC_8H_4O_4$ (M = Mg, Co, Ca, Ba, Sr) [19–22]. Zinc nitrate and sodium terephthalate (NaTPA) were chosen as raw materials. In typical synthesis, 0.01 mol $Zn(NO_3)_2$ and 0.01 mol Na_2TPA were dissolved in 50 ml de-ionized water separately under continuously stirring at room temperature. Afterwards, zinc nitrate solution was added dropwisely into the Na_2TPA solution and white precipitations in hydration form appeared immediately. The mixture was put into a thermostatic drier box at 80 °C for 5 h to insure a complete reaction. Subsequently, the white sediments were centrifuged and washed with water and ethanol for several times. The well-crystalline ZnTPA without crystal water was prepared by annealing ZnTPA·$2H_2O$ at the temperature of 300 °C for 1 h under argon atmosphere. Amorphous phase ZnTPA was formed by heating the crystalline one at 380 °C for 1 h. The hydration form, crystalline form, and amorphous form of zinc terephthalates were denoted as ZnTPA·$2H_2O$, ZnTPA, and ZnTPA-amor, respectively.

2.2. Materials characterization

The phases of ZnTPA·$2H_2O$, ZnTPA and ZnTPA-amor were determined by X-ray powder diffraction (XRD, λ = 1.54056 Å, X'Pert ProMPD) using Cu Kα radiation with a step size of 0.03°. TA instrument Q500 was used in the thermo-gravimetric analysis (TGA) under nitrogen atmosphere at a heating rate of 5 °C from room temperature to 600 °C. A Field emission scanning electron microscope (FEI NanoSEM 430) and Transmission electron microscopy (FEI TecnaiF20 microscope) were applied in morphology characterization. Raman spectroscopy was obtained with a 532 nm wavelength (Renishaw, inVia Reflexg).

2.3. Cell assembling and electrochemical test

The electrodes were prepared with a mixture of 60 wt% active material, 30% carbon black and 10% PVDF binder in slurry form by addition of N-methyl-2-pyrrolidine (NMP) as solvent. Lithium foil was used as the negative electrode and polypropylene (PP) Celgard 2400 membrane was employed as the separator. 1 M $LiPF_6$ dissolved in ethylene carbonate (EC)/diethylene carbonate (DEC)/dimethyl carbonate (DMC) (1:1:1 by volume) was used as the electrolyte. 2032 coin cells were assembled in an argon-filled glove box.

Instrument CT2001A (LAND Electronic Co.) was applied in galvanostatic discharge-charge measurements within the range of 0.2–3.0 V. The cyclic voltammetry (CV) curves were measured by Solartron SI1287 at different scan rates. The powders were pressed into pellets with a thickness of ~0.5 mm and a diameter of 13 mm for the resistance measurements according to the Ohm's law via applying a direct voltage and thus the electronic conductivity can be calculated.

3. Results and discussion

Thermal stability of the as-prepared ZnTPA·$2H_2O$ and ZnTPA has been investigated by thermo-gravimetric analysis (TGA) under nitrogen atmosphere from room temperature to 600 °C (Fig. 1a). It is found that ZnTPA·$2H_2O$ loses weight of 13.4% before 235 °C, which corresponds to a dehydration of 2 crystal water in per formula unit. In line with the anhydrous ZnTPA, the ZnTPA·$2H_2O$ also decomposes at 400 °C, which should finally form zinc oxide and carbon. Its thermal stability is worse than that of CaTPA (~500 °C) [20] and CoTPA (~450 °C) [21]. The phase structure of ZnTPA·$2H_2O$, ZnTPA, and ZnTPA-amor are collected by XRD as displayed in Fig. 1b. According to the Rietveld refinement [23,24], the as-synthesized ZnTPA·$2H_2O$ is a pure phase with C2/c space group (***a*** = 14.922 Å, ***b*** = 5.030 Å, ***c*** = 12.098 Å, ***β*** = 103.82°). This complies with the report of Mark Edgar et al. [25]. After calcination at 300 °C, the anhydrous ZnTPA is obtained with good crystalline. While, there are no reports regarding its phase in the literature. Under a higher annealing temperature at 380 °C, the well-crystalline phase converts into quasi-amorphous phase. In order to well distinguish it from the well-crystalline one, we simply denote the quasi-amorphous as amorphous phase. It is noted that the amorphous phase has no carbon as indicated by a smooth background in XRD and no characteristic carbon peaks in Raman spectroscopy (not shown here). Annealing leading no long range ordered crystal structure is a common phenomenon in the terephthalats (e.g. NiTPA, FeTPA) [26]. Based on the refinement results, the crystallography along [010] direction and molecular structure of ZnTPA·$2H_2O$ are presented in Fig. 1c and d, respectively. Basically, this structure consists of alternative tetrahedral Zn-O inorganic layers and terephthalate organic layers. The inorganic and organic layer distances are 7.50 Å and 6.10 Å, respectively. Different from CoTPA and CaTPA [21,22], the Zn atoms

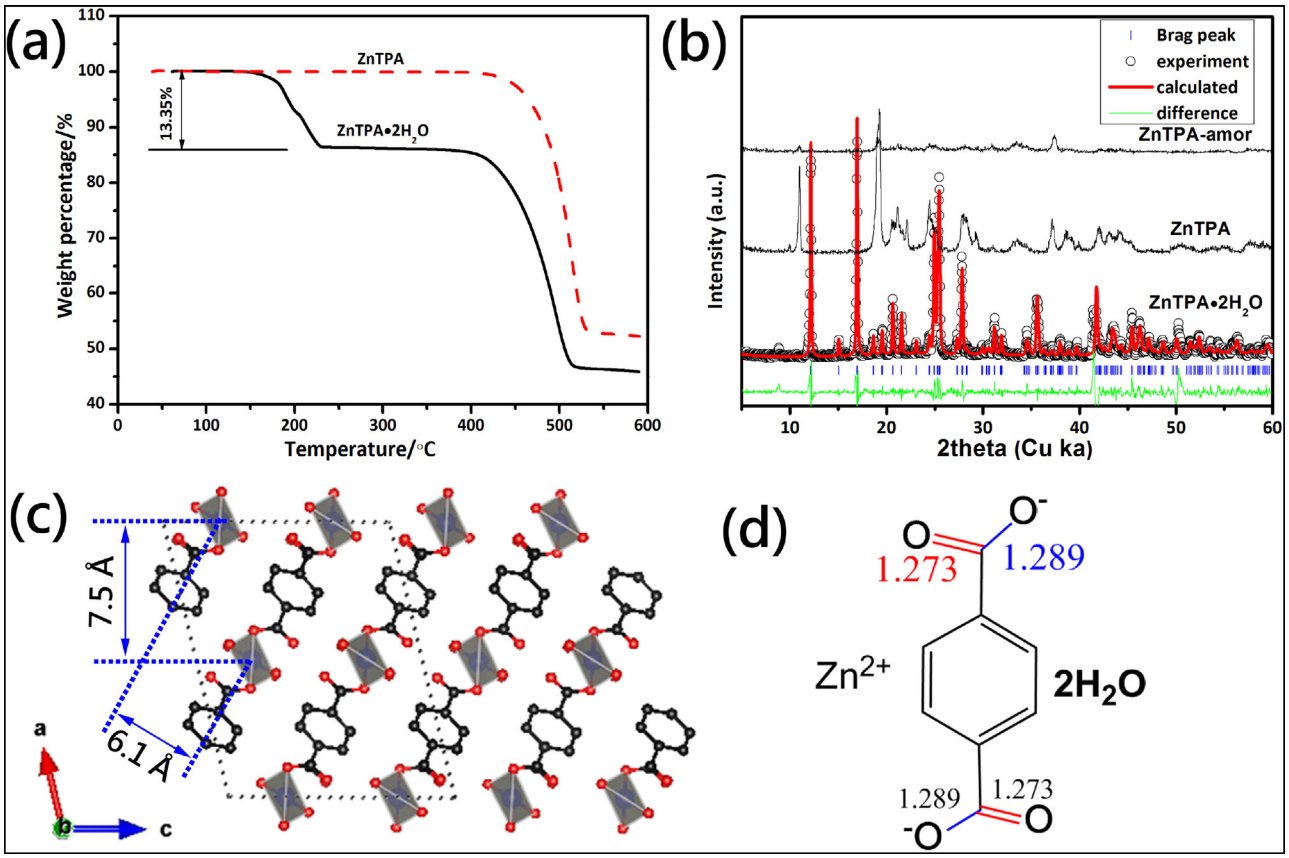

Fig. 1. (a) Thermo-gravimetric analysis of ZnTPA·2H_2O and ZnTPA from RT to 600 °C, (b) XRD patterns and Rietveld refinement with observed data points (red points), calculated data (black line), Bragg positions (green bars) for as-obtained ZnTPA·2H_2O, ZnTPA and ZnTPA-amor, (c) the crystal structure of ZnTPA·2H_2O along the [010] projection. The O, Zn, C atoms are denoted by red, blue, black balls, respectively. H atoms are omitted, (d) Molecular structure of ZnTPA·2H_2O with bond lengths. (For interpretation of the references to colour in this figure legend, the reader is referred to the web version of this article.)

and surrounding O atoms shape in tetrahedron with dangling O atoms rather than octahedrons. The carbonyl groups of C=O and C—O in ZnTPA·2H_2O demonstrate similar bond lengths (1.2730 Å vs. C—O 1.289 Å) indicating a conjugated feature. The —COO— bond lengths vary in different terephthalate salts, which is correlated to their electronegativity and cation radius [20]. Based on its structure and thermal stability, it reveals that ZnTPA is more likely a covalent compound.

The morphology of ZnTPA·2H_2O, ZnTPA, and ZnTPA-amor are visualized by scan electron microscopy (SEM). ZnTPA·2H_2O powders synthesized at 80 °C have particle sizes in the range of 1–20 μm (Fig. 2a). Its morphology can maintain almost unchanged after anhydrous process, revealing that there are no huge volume changes (Fig. 2b). The formed ZnTPA has a sharp and smooth surface suggesting that it has good crystalline and it is confirmed by TEM study (Fig. 1d). After annealing treatment at 380 °C, the long-range ordered phase collapses into smaller size particles (Fig. 1c) and quasi-amorphous phase (Fig. 1e).

The zinc terephthalates were applied as electrode materials for lithium ion batteries with lithium metal foils as counter electrodes. Fig. 3a–c depict the cyclic voltammetry curves for the first four cycles at a scan rate of 0.1 mV s^{-1} in 0.2–3.0 V. All of the three demonstrate a redox couple indexing to absorption/desorption lithium at the electrochemical active carbonyl sites as elucidated in Scheme 1. They share commons that there are quite high current densities in the initial reduction process followed by steady reduction-oxidation current, which gives information of low coulombic efficiency in the first cycle and steady electrochemical performance from the second cycle. As for amorphous zinc terephthalate, it shows the smallest polarization (reduction peak at 0.79 V, oxidation peak at 1.05 V) compared with the other two. Pay attention that the above phenomenon is different from our previous study of Ag_2TPA, CoTPA [18,21], and there is no zinc metallic particles formation in the electrochemical process as absences of a reduction peak for Zn^{2+}/Zn (typically at 1.2 V vs. Li^+/Li) [27] in the cyclic voltammetry (CV). Fig. 3d presents the initial galvanostatic discharge-charge curves at a current rate of 0.5*C* for zinc terephthalates. The theoretical specific capacities for ZnTPA·2H_2O and ZnTPA are 202 mAh g^{-1} and 237 mAh g^{-1}, respectively. Consistent with the CV results, amorphous ZnTPA has the smallest polarization and gives an initial discharge capacity of 626 mAh g^{-1} and a charge capacity of 237 mAh g^{-1}, the corresponding coulombic efficiency (CE) is 38%. This CE is low. It is common in organic electrodes [28–30]. Electrolyte decompositions and formation of SEI, dangling bonds and defect structures as well as its dissolution into the electrolytes can explain this low CE. Optimized the electrode components and the synthesis procedures, surface modification as well as anode prelithiation should be principally improved its CE [31,32].

The ZnTPA·2H_2O and ZnTPA give much lower charge capacity to be 45 mAh g^{-1} and 93 mAh g^{-1}, respectively. It is worth noting that the discharge profiles of the crystalline phase demonstrate a plateau shape ("two-phase" behavior) above 0.45 V, subsequently a slopy shape ("solid solution" behavior). As for the latter, it is suspected that lithium ions are stored in the benzene layers or the grain boundaries [33]. Actually, Armand et al. has also observed this phenomenon in the well-known LiTPA material [8], but gave no detailed explanations. Meanwhile, it is deserved to mention that the crystalline structure of well-crystalline ZnTPA is preserved after cycling evidenced by our XRD (not shown here). The

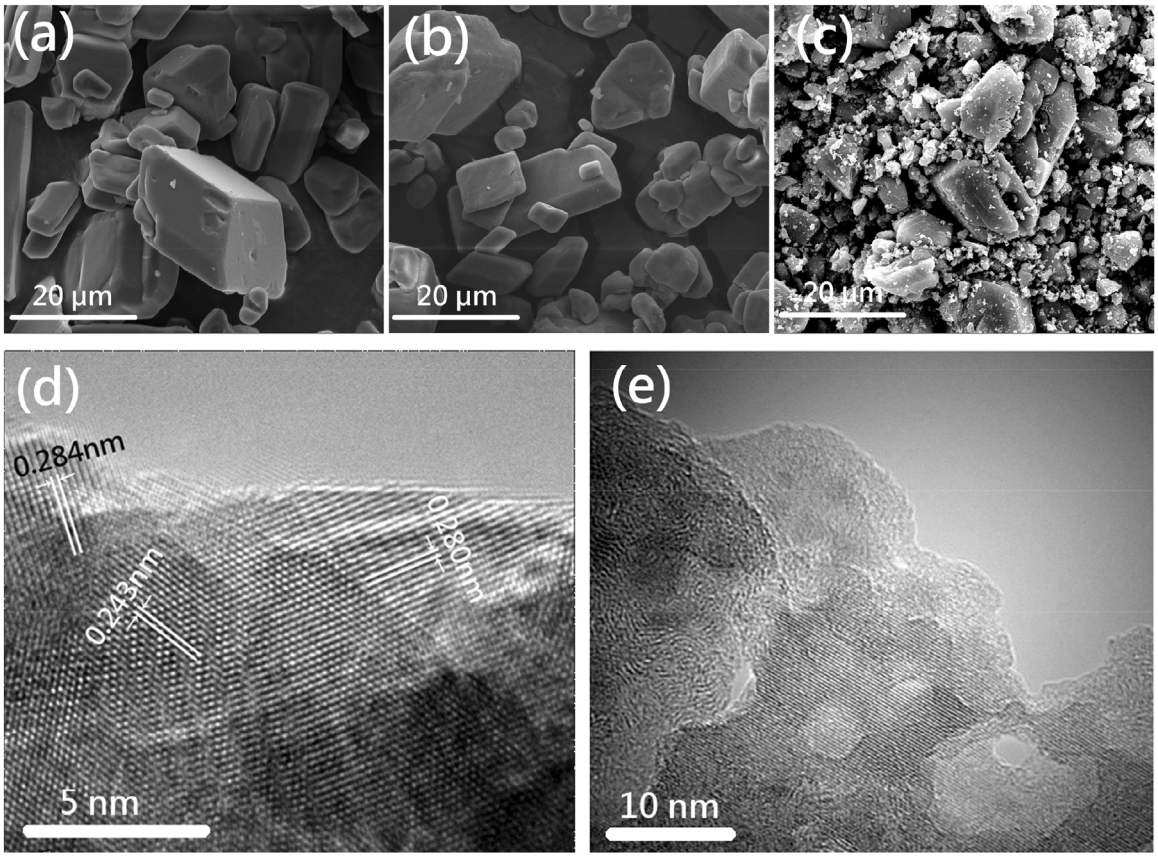

Fig. 2. SEM images of (a) ZnTPA·2H_2O, (b) ZnTPA, and (c) ZnTPA-amor; TEM images of (d) ZnTPA·2H_2O and (e) ZnTPA-amor.

discharge-charge profiles of ZnTPA-amor are different from the crystalline one, which is a solid solution behavior in the whole voltage window. This unique shape seems to be attributed to the amorphous effect as amorphous $LiFePO_4$ and $LiNi_{0.5}Mn_{1.5}O_4$ thin films have also evidenced similar curves [34,35]. The cycling performance of these materials are measured and displayed in Fig. 3e. As the carbon black takes up of 30 wt% in the electrodes, its discharge-charge behavior was herein studied (Fig. 3f). The capacities of zinc terephthalates are presented after deducting the contribution of carbon black with an average capacity of 150 mAh g^{-1} in the voltage window 0.2–3.0 V. The discharge capacity of the ZnTPA-amor remains 180 mAh g^{-1} at 0.5*C* with capacity retention of 66% (100th to 2nd), while the crystalline ZnTPA displays a discharge capacity of 23 mAh g^{-1} at 0.5*C* with capacity retention of only 16% (100th to 2nd). For the ZnTPA·2H_2O, it presents similar cycling performance with the crystalline ZnTPA, which is analogue to the study of CaTPA [22,36]. All of these findings provide that amorphous ZnTPA with chemical bonding type reaction mechanism has the highest capacity and best durable performance. In fact, it is reported that tin-based amorphous oxides also yield a higher capacity than that of crystalline one [37]. While, it is different from the conventional intercalation materials that amorphous structures cause bad electrochemical performance and even electrochemically inert [34,35].

In order to investigate the phases influence on the kinetic performance of zinc terephthalates, electronic conductivities of these three materials are measured. We find that ZnTPA·2H_2O, ZnTPA and ZnTPA-amor have a comparable σ_e, i.e. 5×10^{-7} S m^{-1}, 1×10^{-7} S m^{-1} and 2×10^{-7} S m^{-1}, respectively. Meanwhile, CV experiments with scan rates ranging from 0.1 to 0.4 mV s^{-1} are imported to investigate the lithium ion transportation kinetic behavior, which are shown in Fig. 4. It shows that the peak current (I_p) increases with the increase of scan rates. Meanwhile, with the increase of scan rates, the anodic peaks shift to higher potential, and the cathodic peaks shift to lower potential, which is normally called polarization. Fig. 4 plots the relation between the oxidation peak currents and the square roots of the scan rates ($v^{1/2}$) for these electrodes, which matches a linear relationship very well. This is a typical behavior of diffusion-controlled process rather than electrochemical reaction process. Therefore, the Li-ion diffusion coefficient in the electrodes can be estimated by using Randles–Sevcik equation expressed as [38,39]:

$$I_P = 0.4463 n^{3/2} F^{3/2} C_{Li} S R^{-1/2} T^{1/2} \tilde{D}_{Li}^{1/2} v^{1/2}$$

Where I_p is the peak current, n is the charge transfer number, F is the Faraday constant, C_{Li} is the Li-ion concentration, S is the surface area of the electrode, R is the gas constant, T is the absolute temperature, $\tilde{D}_{Li}$ and v are Li-ion chemical diffusion coefficient and scanning rate, respectively. Thus the chemical diffusion coefficient is proportional to the slope of *Ip* vs. $v^{1/2}$. From the linear slopes, it is obvious that the ZnTPA-amor has the highest apparent Li-ion diffusion coefficient, while the ZnTPA·2H_2O has the lowest apparent Li-ion diffusion coefficient. We believe that amorphous structure provides isotropic lithium diffusion pathway and a short lithium ion diffusion length. According to the equation $D = d^2 t^{-1}$ [40,41], where D is the diffusivity, d is the diffusion distance, and t is the diffusion time, thus a shorter diffusion length results in a square rate higher diffusivity. Moreover, amorphous structure provides a better electrolyte penetration causing better charge-

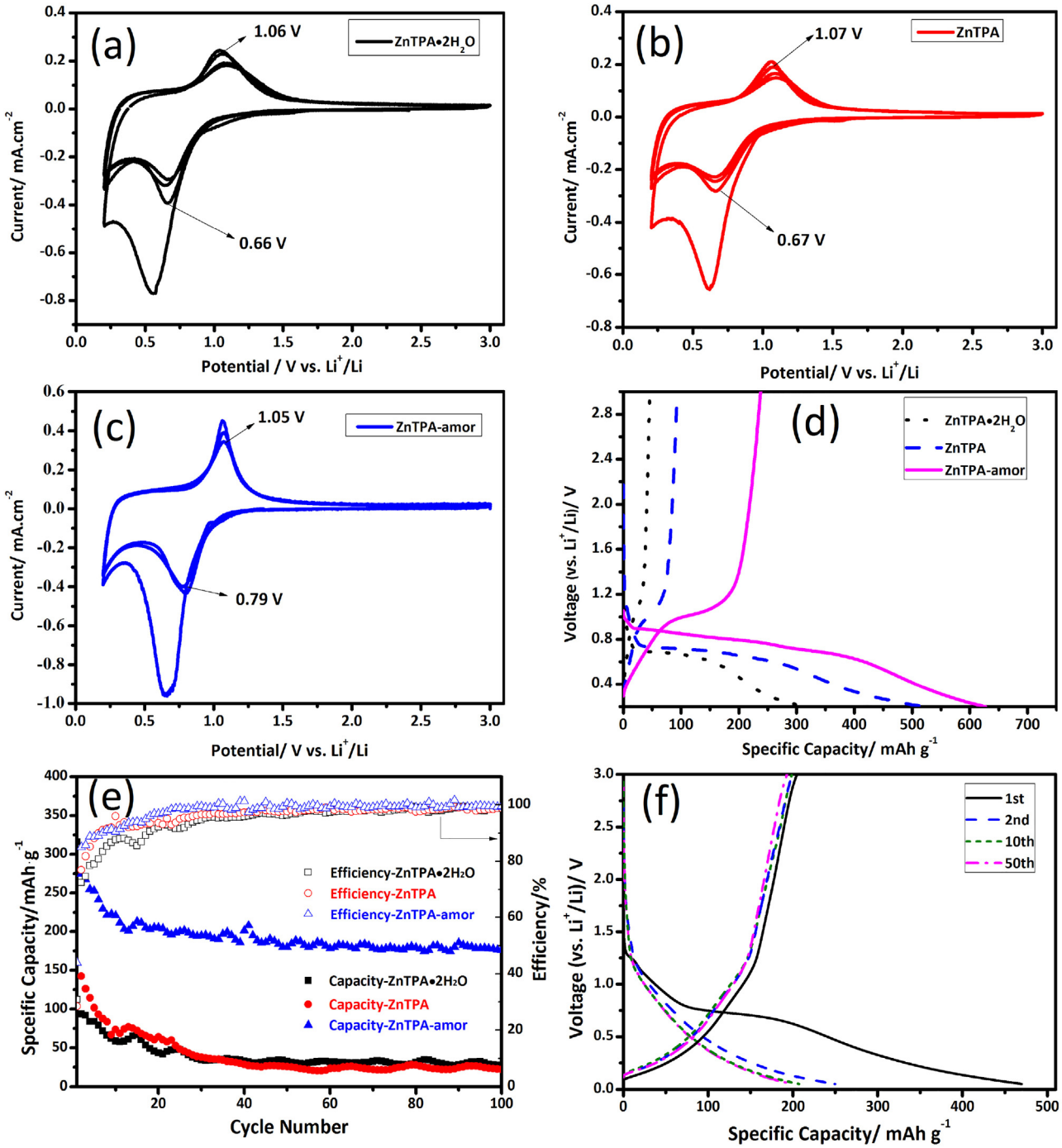

Fig. 3. Cyclic voltammetry (CV) of (a) ZnTPA·2H_2O, (b) ZnTPA, and (c) ZnTPA-amor for the first several cycles at a scan rate of 0.1 mV s^{-1} in the voltage window of 0.2 V–3.0 V, (d) The initial discharge-charge curves and (e) capacity retention behavior of ZnTPA·2H_2O, ZnTPA, and ZnTPA-amor at a current rate of 0.5*C* (2nd to 100th). (f) Galvanostatic discharge-charge profiles for carbon black materials (Electrodes were prepared by 90 wt% carbon black and 10 wt% PVDF).

transfer kinetics between the electrolyte and the electrode materials. All of these contribute to the high lithium ion diffusion coefficient and the good performance of amorphous state ZnTPA.

4. Conclusions

Carbonyl-type organic material zinc terephathalates $ZnC_8H_4O_4$ with well-crystalline and amorphous states are obtained and applied as anodes for lithium ion batteries. The amorphous phase is derived from the crystalline via a simple calcination process at 380 °C. The functional groups —COO— in terephthalates are electrochemical active sites to storage lithium. It is interesting to find that the rate-determine factor for this solid organic materials lies in the lithium ion migration process rather than charge-transfer process. Amorphous $ZnC_8H_4O_4$ with advantages of isotropic and glassy nature presents a much better lithium storage behavior in contrast with crystalline phase including a smaller electrochemical polarization, a higher capacity (180 mAh g^{-1} vs. 25 mAh g^{-1} of crystalline one) and a more durable performance with a higher lithium ion diffusion coefficient although they have

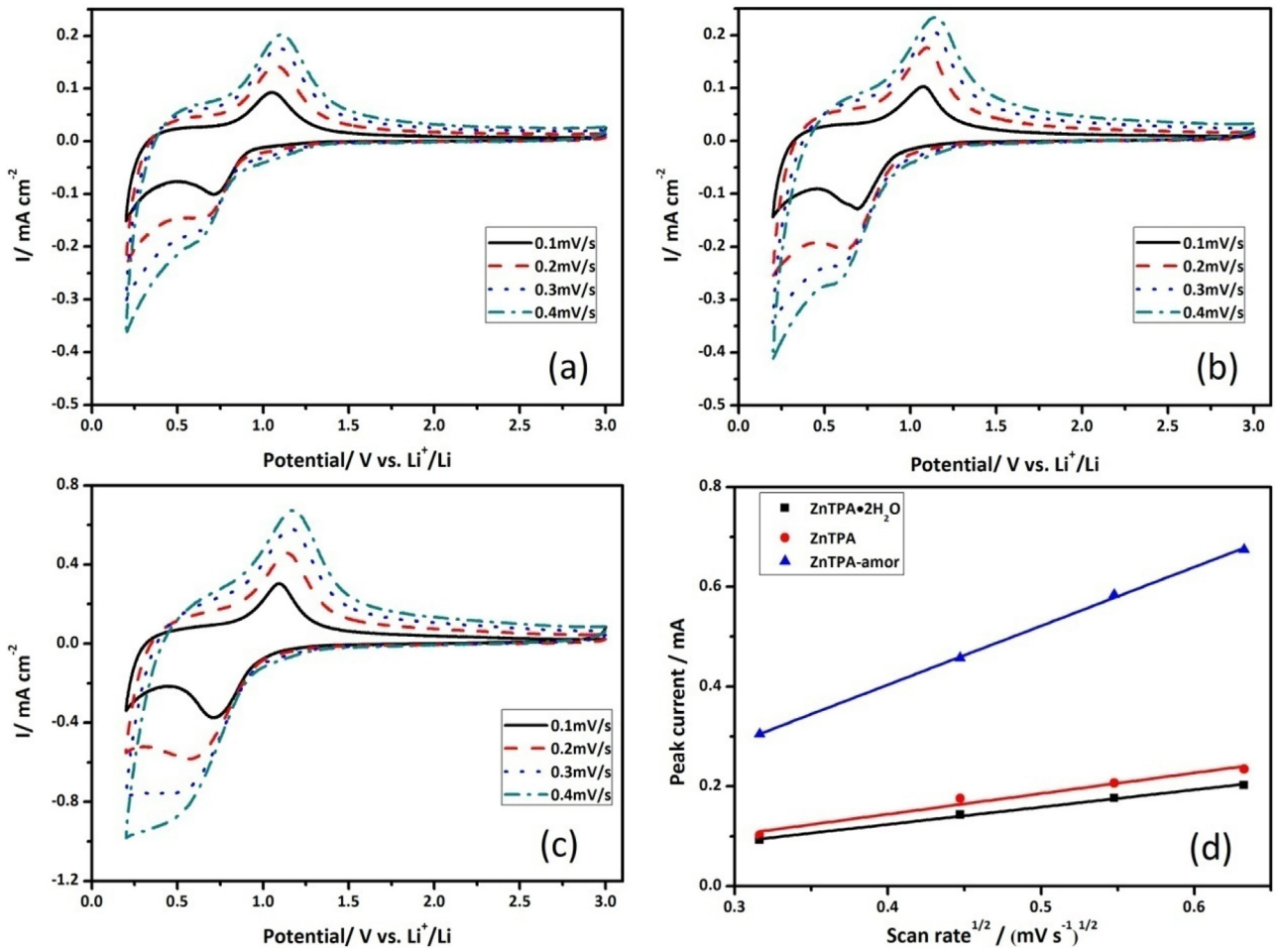

Fig. 4. Evolution of the CV curves as a function of scan rates (from 0.1 to 0.4 mV s^{-1}) for (a) ZnTPA·$2H_2O$, (b) ZnTPA, and (c) ZnTPA-amor, (d) Peak currents against square root of scan rates for ZnTPA·$2H_2O$, ZnTPA, and ZnTPA-amor.

an comparable electronic conductivity of $\sim 10^{-7}$ S m^{-1}. This study demonstrates the importance of engineering the phases to tune the electrochemical performance, which can be extended to other organic electrode materials. It also addresses the importance of solid state ionic subject in the alkaline ion (i.e. Li^+, Na^+, K^+) batteries devices.

Acknowledgements

This work is supported by the National Science Foundation of China (51502032, 21673033, 11234013, 21473022, 51502007). P.G. acknowledges the support from 2011 Program Peking-Tsinghua-IOP Collaborative Innovation Center of Quantum Matter.

References

[1] A.C. Luntz, B.D. McCloskey, Nonaqueous Li-Air Batteries: A Status Report, Chemical Reviews 114 (2014) 11721–11750.
[2] Y. Liang, Z. Tao, J. Chen, Organic Electrode Materials for Rechargeable Lithium Batteries, Advanced Energy Materials 2 (2012) 742–769.
[3] C.-X. Zu, H. Li, Thermodynamic analysis on energy densities of batteries, Energy & Environmental Science 4 (2011) 2614.
[4] X. Wu, S. Jin, Z. Zhang, L. Jiang, L. Mu, Y.-S. Hu, H. Li, X. Chen, M. Armand, L. Chen, X. Huang, Unraveling the storage mechanism in organic carbonyl electrodes for sodium-ion batteries, Science Advances 1 (2015).
[5] S. Renault, D. Brandell, K. Edström, Environmentally-Friendly Lithium Recycling From a Spent Organic Li-Ion Battery, ChemSusChem 7 (2014) 2859–2867.
[6] S. Wu, W. Wang, M. Li, L. Cao, F. Lyu, M. Yang, Z. Wang, Y. Shi, B. Nan, S. Yu, Z. Sun, Y. Liu, Z. Lu, Highly durable organic electrode for sodium-ion batteries via a stabilized a-C radical intermediate, Nature communications 7 (2016) 13318.
[7] J. Xie, C.E. Zhao, Z.Q. Lin, P.Y. Gu, Q. Zhang, Nanostructured Conjugated Polymers for Energy-Related Applications Beyond Solar Cells, Chemistry an Asian journal 11 (2016) 1489–1511.
[8] M. Armand, S. Grugeon, H. Vezin, S. Laruelle, P. Ribiere, P. Poizot, J.M. Tarascon, Conjugateddicarboxylate anodes for Li-ionbatteries, Nature Materials 8 (2009) 120–125.
[9] Y.Y. Zhang, Y.Y. Sun, S.X. Du, H.J. Gao, S.B. Zhang, Organic salts as super-high rate capability materials for lithium-ion batteries, Applied Physics Letters 100 (2012) 091905.
[10] K. Tang, X. Yu, J. Sun, H. Li, X. Huang, Kinetic analysis on LiFePO4 thin films by CV, GITT, and EIS, Electrochimica Acta 56 (2011) 4869–4875.
[11] N. Ogihara, T. Yasuda, Y. Kishida, T. Ohsuna, K. Miyamoto, N. Ohba, Organic Dicarboxylate Negative Electrode Materials with Remarkably Small Strain for High-Voltage Bipolar Batteries, Angewandte Chemie 53 (2014) 11467–11472.
[12] J. Read, A. Driedger, D. Foster, J. Wolfenstine, W. Behl, Low Temperature Performance of λ-MnO2 in Lithium Primary Batteries, Electrochemical and Solid-State Letters 4 (2001) A162.
[13] L. Li, C. Nan, J. Lu, Q. Peng, Y. Li, ChemInform Abstract α-MnO2 Nanotubes: High Surface Area and Enhanced Lithium Battery Properties, Chemical communications 48 (2012) 6945–6947.
[14] Q. Deng, C. Fan, L. Wang, B. Cao, Y. Jin, C.-M. Che, J. Li, Organic Potassium Terephthalate ($K_2C_8H_4O_4$) with Stable LatticeStructure Exhibits Excellent Cyclic and Rate Capability in Li-ion Batteries, Electrochimica Acta 222 (2016) 1086–1093.
[15] Y. Liu, Y. Xu, X. Han, C. Pellegrinelli, Y. Zhu, H. Zhu, J. Wan, A.C. Chung, O. Vaaland, C. Wang, L. Hu, Porous Amorphous FePO4 Nanoparticles Connected by Single-Wall Carbon Nanotubes for Sodium Ion Battery Cathodes, Nano letters 12 (2012) 5664–5668.
[16] Q. Deng, J. Xue, W. Zou, L. Wang, A. Zhou, J. Li, The electrochemical behaviors of $Li_2C_8H_4O_6$ and its corresponding organic acid $C_8H_6O_6$ as anodes for Li-ion batteries, Journal of Electroanalytical Chemistry 761 (2016) 74–79.
[17] Q. Deng, J. Pei, C. Fan, J. Ma, B. Cao, C. Li, Y. Jin, L. Wang, J. Li, Potassium salts of para-aromatic dicarboxylates as the highly efficient organic anodes for low-cost K-ion batteries, Nano Energy 33 (2017) 350–355.
[18] J. Xue, C. Fan, Q. Deng, M. Zhao, L. Wang, A. Zhou, J. Li, Silver Terephthalate ($Ag_2C_8H_4O_4$) Offering in-situ Formed Metal/Organic Nanocomposite as the

Highly Efficient Organic Anode in Li-ion and Na-ion Batteries, Electrochimica Acta 219 (2016) 418–424.
[19] Z. Huang, L. Wang, C. Mou, J. Li, Magnesium Terephthalate as an Organic Anode Material for Sodium Ion Batteries, Acta Physico-Chimica Sinica 30 (2014) 1787–1793.
[20] L. Wang, C. Mou, B. Wu, J. Xue, J. Li, Alkaline Earth Metal Terephthalates MC8H4O4 (M = Ca, Sr, Ba) as Anodes for Lithium Ion Batteries, Electrochimica Acta 196 (2016) 118–124.
[21] L. Wang, M. Zhao, J. Qiu, P. Gao, J. Xue, J. Li, Metal Organic Framework-derived Cobalt Dicarboxylate as a High Capacity Anode Material for Lithium-ion Batteries, Energy Technology (2017), doi:http://dx.doi.org/10.1002/ente.201600424.
[22] L. Wang, C. Mou, Y. Sun, W. Liu, Q. Deng, J. Li, Structure-Property of Metal Organic Frameworks Calcium Terephthalates Anodes for Lithium-ion Batteries, Electrochimica Acta 173 (2015) 235–241.
[23] L. Wang, H. Zhang, Q. Deng, Z. Huang, A. Zhou, J. Li, Superior rate performance of $Li_4Ti_5O_{12}/TiO_2$/C/CNTs composites via microemulsion-assisted method as anodes for lithium ion battery, Electrochimica Acta 142 (2014) 202–207.
[24] L. Wang, J. Xu, C. Wang, X. Cui, J. Li, Y.-N. Zhou, A better understanding of the capacity fading mechanisms of $Li_3V_2(PO_4)_3$, RSC Adv. 5 (2015) 71684–71691.
[25] M. Edgar, R. Mitchell, A.M. Slawin, P. Lightfoot, P.A. Wright, Solid-State Transformations of Zinc 1 4-Benzenedicarboxylates Mediated by Hydrogen-Bond-Forming Molecules, Chemistry-A European Journal 7 (2001) 5168–5175.
[26] H.H. Lee, Y. Park, S.H. Kim, S.-H. Yeon, S.K. Kwak, K.T. Lee, S.Y. Hong, Mechanistic Studies of Transition Metal-Terephthalate Coordination Complexes upon Electrochemical Lithiation and Delithiation, Advanced Functional Materials 25 (2015) 4859–4866.
[27] X. Li, F. Cheng, S. Zhang, J. Chen, Shape-controlled synthesis and lithium-storage study of metal-organic frameworks Zn4O(1 3,5-benzenetribenzoate)2, Journal of Power Sources 160 (2006) 542–547.
[28] J. Wu, X. Rui, G. Long, W. Chen, Q. Yan, Q. Zhang, Pushing Up Lithium Storage through Nanostructured Polyazaacene Analogues as Anode, Angewandte Chemie 54 (2015) 7354–7358.
[29] J. Wu, X. Rui, C. Wang, W.-B. Pei, R. Lau, Q. Yan, Q. Zhang, Nanostructured Conjugated Ladder Polymers for Stable and Fast Lithium Storage Anodes with High-Capacity, Advanced Energy Materials 5 (2015) 1402189.
[30] J. Xie, Z. Wang, P. Gu, Y. Zhao, Z.J. Xu, Q. Zhang, A novel quinone-based polymer electrode for high performance lithium-ion batteries, Science China Materials 59 (2016) 6–11.
[31] J. Xie, X. Rui, P. Gu, J. Wu, Z.J. Xu, Q. Yan, Q. Zhang, Novel Conjugated Ladder-Structured Oligomer Anode with High Lithium Storage and Long Cycling Capability, ACS applied materials & interfaces 8 (2016) 16932–16938.
[32] L. Wang, Z. Schnepp, M.M. Titirici, Rice husk-derived carbon anodes for lithium ion batteries, Journal of Materials Chemistry A 1 (2013) 5269–5273.
[33] M.A. Sk, S. Manzhos, Exploring the sodium storage mechanism in disodium terephthalate as anode for organic battery using density-functional theory calculations, Journal of Power Sources 324 (2016) 572–581.
[34] K. Tang, J. Sun, X. Yu, H. Li, X. Huang, Electrochemical performance of $LiFePO_4$ thin films with different morphology and crystallinity, Electrochimica Acta 54 (2009) 6565–6569.
[35] L. Wang, H. Li, M. Courty, X. Huang, E. Baudrin, Preparation and characterization of $LiNi_{0.5}Mn_{1.5}O_{4-\delta}$ thin films taking advantage of correlations with powder samples behavior, Journal of Power Sources 232 (2013) 165–172.
[36] L. Wang, H. Zhang, C. Mou, Q. Cui, Q. Deng, J. Xue, X. Dai, J. Li, Dicarboxylate $CaC_8H_4O_4$ as a high-performance anode for Li-ion batteries, Nano Research 8 (2015) 523–532.
[37] Y. Idota, Tin-Based Amorphous Oxide: A High-Capacity Lithium-Ion-Storage Material, Science 276 (1997) 1395–1397.
[38] L. Wang, J. Bai, P. Gao, X. Wang, J.P. Looney, F. Wang, Structure Tracking Aided Design and Synthesis of $Li_3V_2(PO_4)_3$ Nanocrystals as High-Power Cathodes for Lithium Ion Batteries, Chemistry of Materials 27 (2015) 5712–5718.
[39] X. Dai, L. Wang, J. Xu, Y. Wang, A. Zhou, J. Li, Improved Electrochemical Performance of $LiCoO_2$ Electrodes with ZnO Coating by Radio Frequency Magnetron Sputtering, ACS Applied Materials & Interfaces 6 (2014) 15853–15859.
[40] P. Gao, L. Wang, Y.Y. Zhang, Y. Huang, L. Liao, P. Sutter, K. Liu, D. Yu, E.G. Wang, High-Resolution Tracking Asymmetric Lithium Insertion and Extraction and Local Structure Ordering in SnS_2, Nano Letters 16 (2016) 5582–5588.
[41] P. Gao, Y.-Y. Zhang, L. Wang, S. Chen, Y. Huang, X. Ma, K. Liu, D. Yu, In situ atomic-scale observation of reversible sodium ions migration in layered metal dichalcogenide SnS_2 nanostructures, Nano Energy 32 (2017) 302–309.